Vortex Suppression on High Subsonic Turbine Blade via Micro Holes (30 Degree)

Mohd Hafiz Mohd Noh, Ahmad Hussein Abdul Hamid*
Faculty of Mechanical Engineering, UiTM Shah Alam Malaysia
**mhafiz_noh@yahoo.com*

Koichi Moris
Department of Aerospace Engineering, Nagoya University Japan

ABSTRACT

The vortex shedding of a turbine blade is suppressed by making a hole, connecting between the pressure side and suction side in the area of the trailing edge. Computational simulation has been done via numerical code by using Spalart–Allmaras turbulence model with Delayed Detached Eddy Simulation. The exit Reynolds number is 2.8×10^6 and the exit isentropic Mach number is 0.79. The size of the hole is 0.094D with a connecting angle of 30 degrees. The result shows that the vortex has successfully been suppressed at the turbine trailing edge and turbine wake area. The micro-hole is capable to reduce initial vortex formation which can be confirmed by the decrement of frequency peak and via observation of flow field vortex simulation.

Keywords: *Turbine Blade; Flow Field; Numerical Investigation; Vortex Shedding; Pressure Distribution*

Introduction

The unsteady phenomenon at turbine blade wake is normally represented in the form of vortex shedding. At higher subsonic conditions, this vortex shedding is very significant and devotes the losses, which contributes approximately $1/3^{rd}$ of blade profile loss. Major losses in turbine blades include primary loss (due to boundary layer), shock loss (due to oblique or normal shock which occurs at the trailing edge), and mixing losses (due to wake rapid dissipation). These losses can be decreased by modifying the respective blade

ISSN 1823-5514, eISSN 2550-164X

Received for review: 2021-05-29
Accepted for publication: 2021-11-15
Published: 2022-01-15

geometry and by controlling the flow control via active flow control, passive flow control, and hybrid (combination between active and passive flow control).

A lot of research has been dedicated to flow control in a turbine blade. Li et al. have successfully controlled the separation on Low-Pressure Turbine blades by combining steady vortex generator jets and deflected trailing edges [1]. Furthermore, a micro single dielectric barrier discharge (SDBD) with micro linear plasma synthetic jets (L-PSJ) has given a reduction of recirculation and decreased the boundary layer thickness of a turbine blade [2]. Tranficante et al. have conducted a study on flow separation control on a compressor-stator cascade using three different methods - plasma actuator, synthetic jets and continue jets [3]. Plasma actuator is very good in controlling the downstream flow separation, while synthetic jets actuator is very good in terms of pressure loss reductions [3]. This finding is also supported by Xin et al. whereby turbulent boundary layer separation of a wing can be suppressed by using a plasma actuator [4].

For passive flow control, the application of dimpled surface on turbine blade has proven to be effective on drag reduction and flow separation loss [5,6]. Wang et al. have installed a micro-blade at upstream onset separation location of compressor cascade and the result shows the formation of a jet has reduced the boundary layer thickness on the suction surface [7]. Reduction in trailing edge noise also leads to reduction on surface pressure spectra, which at the same time decreases pressure fluctuation in the mid-frequency region [8]. Zhou et al. investigated the effect of the trailing edge thickness on vortex shedding and found that the increment between 1.4% to 2.8% of trailing edge thickness shows the reduction in the turbine blade losses [9].

In this paper, the result for making a hole with an inclination angle of 30 degrees between the pressure side and suction side at the trailing area has been presented. This connection may create a phenomenon of blowing and suction between both sides as agreed by [10]. A suction slot on the blade can reduce the total pressure loss while the blowing phenomenon can improve the pressure distribution on the blade [11,12]. The location and size of the hole were not optimized, with limited span size, the number of holes has been fixed to be eight (8) and the size of the hole is 0.094 trailing edge diameter D.

Numerical computational setup

The configuration of the blade is presented in Table 1 and further illustrated in Figure 1. The numerical model consists of the continuity equation, three dimensional Navier-Stokes equations for unsteady compressible flow.

Table 1: Blade configuration

Chord Length, C	140 mm
Axial Chord Length, C_{ax}	91.84 mm
Pitch, s	97.44 mm
Span	14 mm
Trailing Edge Diameter, D	7.48 mm

The in-house code being used in this calculation is single block and second-order accurate in time. The inviscid fluxes are discretized using the total variation diminishing scheme and viscous fluxes are discretized using standard central differences. Roe's flux-difference splitting scheme is used for a numerical inviscid flux calculation, where second-order accuracy is achieved employing the MUSCL scheme with the van Albada flux limiter. The lower upper symmetric Gauss-Seidel together with a second-order dual time-stepping method is employed to calculate the unsteady flow. Figure 2 shows the $\pm S/D$ measurement, where S is defined as the trailing edge length and the definitions of x/D and Y/D. Time marching implicit scheme being calculated with five inner interactions with the maximum number of 2 x 10^6 with a CFL value of 10.

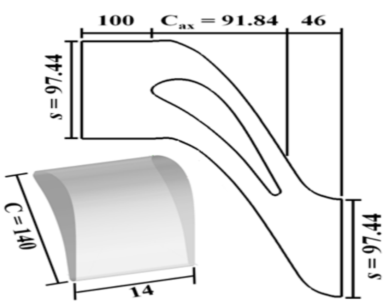

Figure 1: Blade configuration (in mm).

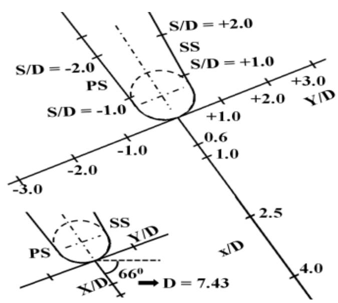

Figure 2: Definition of *S/D, x/D,* and *Y/D.*

Boundary conditions and turbulence model

An O-type structured grid with 4000000 points has been used in this calculation. The closes distance from the wall to the first grid is 0.002 mm, which gives an equivalent value of y+ ≈1. On the blade surface, a non-slip adiabatic wall boundary condition is applied. Subscripts *"01*" and "*02*" refer to the inlet and outlet condition, while subscripts "*in*" and "*out*" represent inside and outside the calculation domain. At the inlet, subsonic Riemann Invariant condition, R_{01} has been imposed with inlet total pressure of 140 kPa and total temperature of 280 K. A periodical boundary condition is applied for this calculation [13,14]. At the outlet, the isentropic Mach number of 0.79, and the Reynolds number is 2.8 x 10^6 being imposed [15, 16]. The static pressure of P_{02} = 92.755 kPa has been set, with subsonic outlet boundary condition and entropy relation have been applied and outlet subsonic Riemann Invariant condition, R_{02} being imposed.

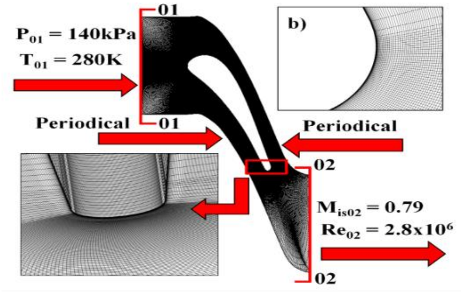

Figure 3: Detail all the boundary conditions and O-type grid.

Since the hole size is very small (0.094D), so the flow inside the hole is not being simulated, and we can assume that the flow inside the hole is to be laminar, incompressible, and uniform. Each micro-hole is modeled using the Hagen–Poiseuille equation [17], where this equation is involved in mass, momentum, and energy calculation;

$$U = \frac{R^2}{4\mu}\left[-\frac{\Delta P}{\Delta L}\right] \tag{1}$$

where U is the velocity through the hole, R is the radius of the hole, μ is the dynamic viscosity, ΔP is the pressure difference between the pressure side and suction side and ΔL is the hole length.

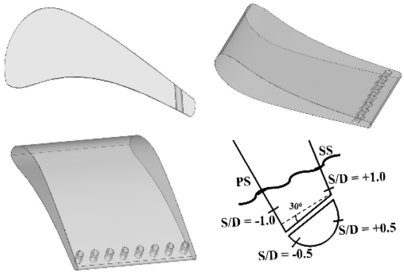

Figure 4: 30 degree connected holes on the blade.

Equation (1) is widely used in morphology and biology [17,18]. Besides, this equation is also being applied to the research on insect fluid feedings [19]. After validation, the micro-hole is applied in the area of the trailing edge of the studied blade as illustrated in Figure 4. The Spalart Allmaras viscosity, $\tilde{v}$ model equation can be expressed as;

$$\begin{aligned}\frac{D\tilde{v}}{Dt} &= \underbrace{c_{b1}\tilde{S}\tilde{v}}_{Production} \\ &+ \underbrace{\frac{1}{\sigma}\left[\nabla.\left((\nu+\tilde{v})\nabla\tilde{v}\right) + c_{b2}(\nabla\tilde{v})^2\right]}_{Diffusions} \\ &- \underbrace{c_{w1}f_w\left(\frac{\tilde{v}}{d}\right)^2}_{Destruction}\end{aligned} \quad (2)$$

subscript *b* here stands for basic, *d* is the characteristic length, $\tilde{S}$ is local deformation rate, υ is molecular viscosity, $\tilde{v}$ is the working variable [20]. Further information has been explained in the references [20, 21]. *DES* (Detached Eddy Simulation) has changed the characteristic length *d* with:

$$\tilde{d} = (\ d, \Delta C_{DES}) \quad (3)$$

where Δ are local maximum grid spacing with C_{DES} is equal to 0.65. This *DES* $\tilde{d}$, is purposely to recalculate eddy viscosity, where at the distance close to the wall, $\tilde{d}$ will be defined as *d* and other domain regions will be defined as $\tilde{d} = \Delta C_{DES}$. For simulation calculation on turbine blade related, the possibility of a boundary layer is less than minimum grid size, which frequently happens since d is grid size-dependent. To overcome this, *DDES* (Delayed Detached Eddy Simulation) has added parameter r_d in the basic Spalart–Allmaras model [22]

$$f_d = 1 - tanh\ tanh\ (\ [8r_d]^3) \quad where\ r_d = \frac{\upsilon_T + \upsilon}{\sqrt{u_{ijk}u_{ijk}\kappa^2 d^2}} \quad (4)$$

where u_{ijk} is velocity profile and f_d is 1 in the Large Eddy Simulation (*LES)* region, and $r_d \ll 1$ and equal zero in the Reynolds Average Navier-Stokes (RANS) region [22]. κ is von Karman constant (0.41) and υ_T is kinematic eddy viscosity. d_{DES} which is a new calculation for characteristic length for *DDES* can be expressed as;

$$d_{DES} = d - f_d(\ 0, d - C_{DES}\Delta) \quad (5)$$

For this new d_{DES}, the calculation ($f_d = 0$) will be based on length scale, and for others, it will behave as a basic DES model calculation.

Result and Findings

Validation with experiment

Figure 5 shows the simulation result of DES and DDES turbulence compared with experimental data obtained by Sieverding et al. [15, 16]. DES turbulence model cannot capture the primary three pressure minima observed in the experiment at the location of S/D ≈ −0.7, 0.0, and 0.75. This is believed due to grid size on DES model destruction part particularly smaller than boundary layer [22]. However, *DDES* turbulence model can capture three locations of minimal pressure, which is prove that the influence of length scale solution in turbomachinery is very important. As the result, *DDES* turbulence model has been chosen, which is also in line with Bernadini et al. [21].

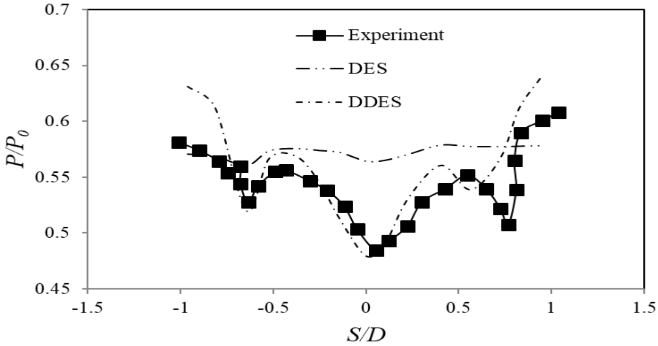

Figure 5: Dimensionless pressure distribution comparison between DES turbulence model, DDES turbulence model with the experiment result.

This is also supported by Magagnato et al. in their finding, which shows that *DDES* turbulence model was able to trace the transitional separation flow on turbine blade simulation [23]. Melzer et al. reported phenomena of trailing edge vortex shedding at *te/o* = 7.8%, which shows that this area is an important area for initial vortex formation, which leads to a very fine grid in computational simulation to capture this situation [24]. All minima dimensionless pressure value has been captured on DDES turbulence model, and we can observe some differences at $|S/D| > 0.8$. This is different mainly due to overexpansion separation plateau [15].

Figure 6 shows the isentropic Mach number around the blade. There is no significant difference between each result. This proves that there is almost no vortex shedding or fluctuation occurring at a higher value of S/D of turbine blade trailing edge, which leads to the direction of this research to focus on the trailing edge area. This result also shows that the numerical result has been successfully validated with the experiment data.

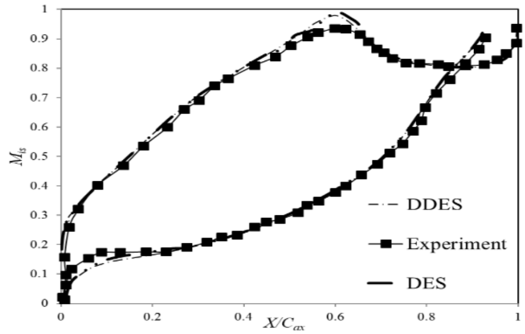

Figure 6: The result of isentropic Mach number around the blade between simulation and experiment.

The results are further validated by comparing in terms of boundary layer profile at the pressure side of the trailing edge area. Again, we can see *DES* cannot capture velocity magnitude near the wall especially at 0.0 mm < y < 0.4 mm region, this may due to length scale calculation. On the other hand, DDES has shown very good agreement with the experiment data as in Figure 7.

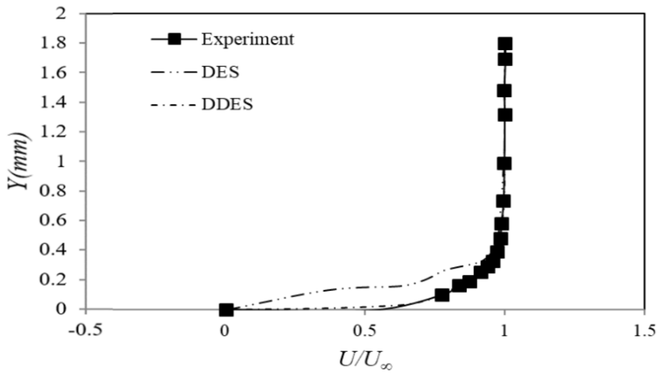

Figure 7: Dimensionless velocity profiles

The application of micro-hole

The location of the micro-hole has been fixed at S/D = -0.62. This location has been chosen due to the higher dominant frequency at this particular area. Figure 8 shows the comparison of Fast Fourier Transformation (FFT) calculation for the hole and based case (no hole configuration) at the location of S/D = -0.62. As you can see, when the micro-hole has been applied at the respective area, the frequency has been reduced significantly and the third frequency peak has almost been eliminated. The first peak was recorded approximately at 7.46 kHz while the second peak hit at approximately 14.84 kHz.

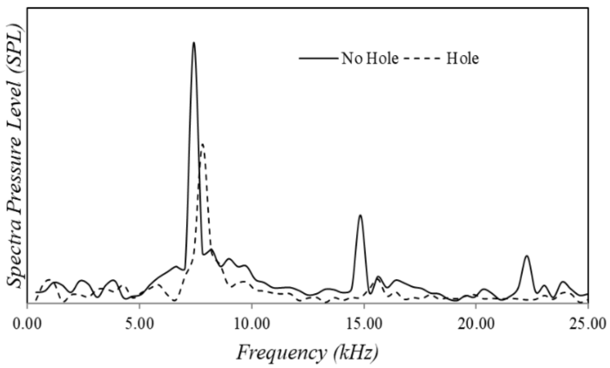

Figure 8: Pressure spectra comparison between hole and no hole configuration at *S/D* = -0.62.

The instantaneous iso-surface vorticity of the study case has been plotted to show better comparison (in terms of flow field) between the base case (no hole) and hole case in a complete cycle vortex manner (same time phase). The three-dimensional view has been oriented, to observe the initial vortex performance near the hole on the blade trailing edge. Figure 9 (i) shows the initial condition of wake vortex formation for no hole and hole cases. For the base case, at approximately (S/D = -0.62) area, the strong vortex has been induced at the surface of the trailing edge. As the series of micro-hole being applied, the vortex has successfully suppressed as the contour and the physical structure of the respective vortex has been changed, which indicates the suppression phenomena has occurred. Adding holes shows the vortex has been suppressed even at an early stage and also reduced the vortex concentration at this area. Suppressing the initial formation of the vortex will influence the following vortex formation. This can be observed further downstream of the blade as stipulated in Figure 9 (ii).

Further downstream, the vortex continues to induce from the trailing edge of the turbine blade for both cases, as the hole case produced see less strong has been produced as compared with the based case (Figure 9 (ii)). The second and third vortices downstream of the blade also showed different shapes between the base case and hole case, which the base case produced relatively greater vortices as compared with the hole case. This is the outcome fact for the vortex from the pressure side started to enter and mix with suction side vortex. The 30-degree inclination connected hole has shown a significant effect on the suction side which shows less strong vortices than the pressure side.

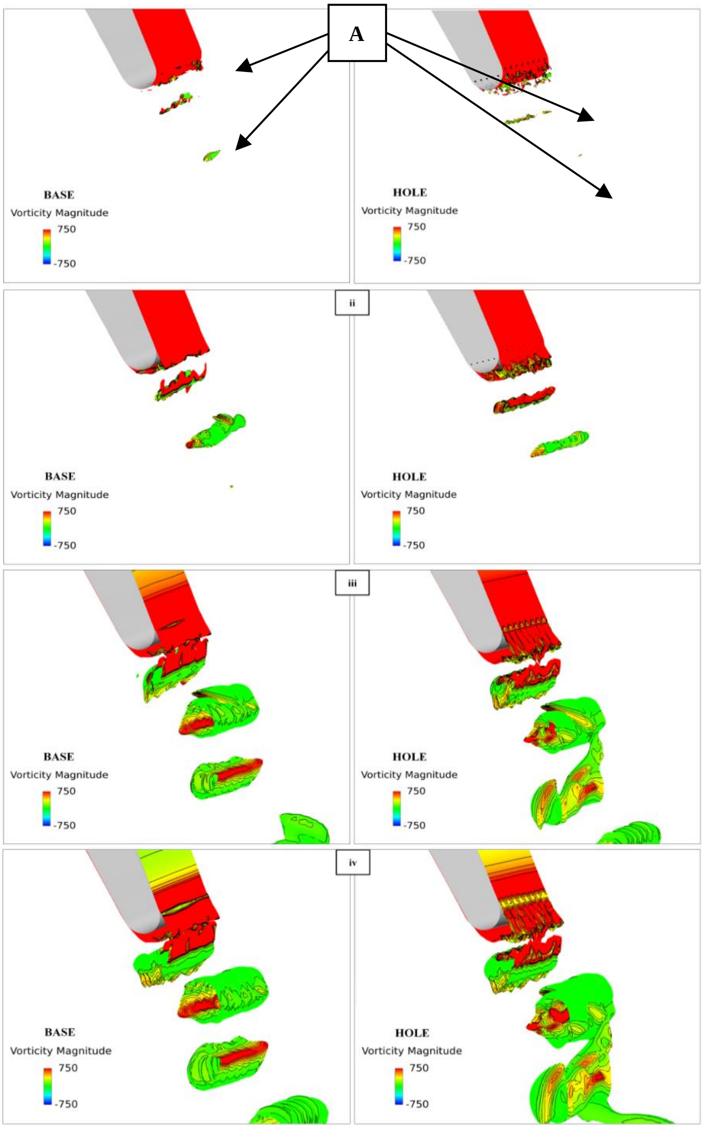

Figure 9: Instantaneous vorticity magnitude comparison.

The inclination has made the vortex from the pressure side enroll "earlier" than the suction side and make the mix interaction between both vortexes settled more biased to the suction side, which leads for the result for more steady vortex formation on the surface. As the initial vortex has been suppressed on the hole case, this also leads to delay from break up into second vortices lead. In the base case, this delayed phenomenon did not appear, and the strong vortex has broken up earlier. The delay on the hole case is believed to be a reason why fewer secondary strong vortex was produced on the trailing edge downstream. Also, on the hole case, further downstream vortices are observed to be separated from the initial vortex, which these phenomena did not happen on the base case. The vortex shedding growth at the wake and for hole case, this growth has been significantly reduced, which has been labeled as "A" in Figure 9 (iii).

The vortex continues to induce in Figure 9 (iv). Downstream vortices continue to suppress but in the base case, the vortex did not separate at all. At the hole area, even more stronger vortex produced on hole case as compared with the based case, the vortex seems to be well distributed (in span-wise direction), which lead to delayed formation downstream the blade.

Conclusion

The proposed method by connecting between the suction side and pressure side of a turbine blade has successfully suppressed the vortex at the trailing edge and wake area. Added a series of micro-holes has capable to reduce initial vortex formation, which can be confirmed by decrement of frequency peak and also via observation of vortex simulation.

References

[1] C. Li, P. Yan, X. Wang, W. Han, and Q. Wang, "Numerical study of combining steady Vortex Generator Jets and Deflected Trailing edge to reduce the blade numbers of low pressure turbine stage," *Journal of Thermal Science*, vol. 25, no. 6, pp. 511–517, 2016.

[2] M. G. De Giorgi, A. Ficarella, F. Marra, and E. Pescini, "Micro DBD plasma actuators for flow separation control on a low pressure turbine at high altitude flight operating conditions of aircraft engines," *Applied Thermal Engineering*, vol. 114, pp. 511–522, 2017.

[3] S. Traficante, M. G. De Giorgi, and A. Ficarella, "Flow Separation Control on a Compressor-Stator Cascade Using Plasma Actuators and Synthetic and Continuous Jets," *Journal of Aerospace Engineering*, vol. 29, no. 3, pp. 04015056, 2016.

[4] X. Zhang, Y. Huang, X. Wang, W. Wang, K. Tang, and H. Li, "Turbulent boundary layer separation control using plasma actuator at Reynolds number 2000000," *Chinese Journal of Aeronautics*, vol. 29, no. 5, pp. 1237–1246, 2016.

[5] M. van Nesselrooij, L. L. M. Veldhuis, B. W. van Oudheusden, and F. F. J. Schrijer, "Drag reduction by means of dimpled surfaces in turbulent boundary layers," *Experiments in Fluids*, vol. 57, no. 9, 2016.

[6] P. W. Bearman and J. K. Harvey, "Control of circular cylinder flow by the use of dimples," *AIAA Journal*, vol. 31, no. 10, pp. 1753–1756, 1993.

[7] B. Wang and Y. Wu, "Passive flow control of the corner separation in an annular compressor cascade with a micro-blade," *Proceedings of the Institution of Mechanical Engineers, Part A: Journal of Power and Energy*, vol. 233, no. 3, pp. 293–308, 2018.

[8] Szoke, M., and Azarpeyvand, M., "Active Flow Control Methods for the Reduction of Trailing Edge Noise", *in 23rd AIAA/CEAS Aeroacoustics Conference*, Colorado, 5-9 June 2017.

[9] C. Zhou, H. Hodson, and C. Himmel, "The Effects of Trailing Edge Thickness on the Losses of Ultrahigh Lift Low Pressure Turbine Blades," *Journal of Turbomachinery*, vol. 136, no. 8, 2014.

[10] M. M. El-Gendi, M. K. Ibrahim, K. Mori, And Y. Nakamura, "Novel Flow Control Method for Vortex Shedding of Turbine Blade," *Transactions of The Japan Society for Aeronautical and Space Sciences*, Vol. 53, No. 180, pp. 122–129, 2010.

[11] Y. Liu, J. Sun, and L. Lu, "Corner Separation Control by Boundary Layer Suction Applied to a Highly Loaded Axial Compressor Cascade," *Energies*, vol. 7, no. 12, pp. 7994–8007, 2014.

[12] Kurmanov, B., Namba, M., and Podvidz, G., "Turbulent Flow Computation in Film-Cooling Turbine Cascade", *in Proceedings of the International Gas Turbine Congress 2003, Tokyo*, 2003.

[13] Azebedo, M.A., Cavadas, A.S., Coelho, P.M., Proenca M.F., and Pinho, F.T., "Control of vortex shedding behind a circular cylinder at moderate Reynolds number", *in Conferência Nacional em Mecânica dos Fluidos, Termodinâmica e Energia*, pp.1-9, 2012.

[14] G. Cerri, A. Giovannelli, L. Battisti, and R. Fedrizzi, "Advances in effusive cooling techniques of gas turbines," *Applied Thermal Engineering*, vol. 27, no. 4, pp. 692–698, 2007.

[15] C. H. Sieverding, D. Ottolia, C. Bagnera, A. Comadoro, J.-F. . Brouckaert, and J.-M. Desse, "Unsteady Turbine Blade Wake Characteristics," *Journal of Turbomachinery*, vol. 126, no. 4, pp. 551–559, 2004.

[16] C. H. Sieverding, H. Richard, and J.-M. Desse, "Turbine Blade Trailing Edge Flow Characteristics at High Subsonic Outlet Mach Number," *Journal of Turbomachinery*, vol. 125, no. 2, pp. 298–309, 2003.

[17] H. H. Lipowsky, S. Kovalcheck, and B. W. Zweifach, “The distribution of blood rheological parameters in the microvasculature of cat mesentery.,” *Circulation Research*, vol. 43, no. 5, pp. 738–749, 1978.

[18] C. Loudon and K. McCulloh, “Application of the Hagen—Poiseuille Equation to Fluid Feeding through Short Tubes,” *Annals of the Entomological Society of America*, vol. 92, no. 1, pp. 153–158, 1999.

[19] P. C. Andersen, B. V. Brodbeck, and R. F. Mizell, “Feeding by the leafhopper, Homalodisca coagulata, in relation to xylem fluid chemistry and tension,” *Journal of Insect Physiology*, vol. 38, no. 8, pp. 611–622,1992.

[20] Spalart, P.R., Jou,W.-H., Strelets, M., and Allmaras, S.R., “Comments on the feasibility of LES for wings, and on a hybrid RANS/LES approach”, *in Advances in DNS/LES: Proceedings of the First AFOSR International Conference on DNS/LES, Louisiana Tech University*, Ruston, Louisiana, USA, August 4-8, 1997.

[21] C. Bernardini, M. Carnevale, M. Manna, F. Martelli, D. Simoni, and P. Zunino, “Turbine blade boundary layer separation suppression via synthetic jet: An experimental and numerical study,” *Journal of Thermal Science*, vol. 21, no. 5, pp. 404–412, 2012.

[22] M.El-Ghondour, Shatat, M.M.E., and Nakamura, Y., “On the physics of Vortex Formation at the Tip of a Turbine Blade”, *in ASME Turbo Expo 2012: Turbine Technical Conference and Exposition*, June 11-15, 2012.

[23] Magagnato, F., and Gabi, M., “Prediction of Transitional Flow of Turbine Blades with DDES and LES”, *in Proceedings of 8th World Congress on Computational Mechanics*, July, 2008.

[24] Melzer, A.P., and Pullan, G., “The Role of Vortex Shedding in the Trailing Edge of Transonic Turbine Blade”, *Proceedings of the ASME Turbo Expo 2018: Turbomachinery Technical Conference and Exposition. Volume 2B: Turbomachinery.* Oslo, Norway. June 11–15, 2018.